Int J Adv Manuf Technol (2016) 87:2099–2111
DOI 10.1007/s00170-016-8596-2

ORIGINAL ARTICLE

Development of a double-frequency elliptical vibration cutting apparatus for freeform surface diamond machining

Xiaoqin Zhou[1] · **Chengming Zuo**[1] · **Qiang Liu**[1] · **Rongqi Wang**[1] · **Jieqiong Lin**[2]

Received: 8 July 2015 / Accepted: 2 March 2016 / Published online: 18 March 2016

Abstract A new apparatus is proposed for the freeform surface diamond machining on die steel in this paper. Fast tool servo-based diamond turning is considered to be the most effective and efficient generating technology for freeform surfaces, but freeform surfaces of die steel cannot be machined very effectively by this technology because of the severe tool wear and the surface quality degradation. Elliptical vibration cutting has demonstrated excellent performances in machining die steel materials. Therefore, this paper proposes a double-frequency elliptical vibration cutting apparatus, which combines fast tool servo and elliptical vibration cutting. The device is designed to be a flexure hinge structure and driven by two piezoelectric actuators to generate tool motions. A series of testing experiments are conducted, in which the device performs well. In addition, the freeform surfaces are generated on the 40Cr die steel workpieces with the device, and the surface machined by double-frequency elliptical vibration cutting shows much better surface integrity and form accuracy than the surface machined by conventional fast tool servo, which validates the principle and the proposed apparatus.

Keywords Freeform surfaces · Fast tool servo · Elliptical vibration cutting · Die steel · Double-frequency elliptical vibration cutting

✉ Qiang Liu
liu-qiang-1111@163.com

[1] School of Mechanical Science and Engineering, Jilin University, Changchun 130022, People's Republic of China

[2] School of Electro-Mechanical Engineering, Changchun University of Technology, Changchun 130012, People's Republic of China

1 Introduction

Freeform surfaces have been widely used in various fields, such as aerospace, new energy, and biomedical engineering [1]. Fast tool servo (FTS)-based diamond turning [2, 3] has been considered to be the most effective and efficient technology for the freeform surface machining. Freeform surfaces of die steel are widely used in the fabrication of molds and mechanical components. Whereas these freeform surfaces cannot be machined very effectively by the FTS diamond turning technology, because die steel materials cannot be directly machined using diamond tools [4]. Paul et al. [5] found that the chemical reaction between diamond and ferrous materials causes severe chemical wear of diamond tools. In addition, the chemical wear accelerates the mechanical abrasion of the tools, which results in the significant deterioration of the machined surfaces. Li et al. [4] reviewed the main technologies and strategies for the reduction of tool wear, such as vibration-assisted machining, cryogenic cutting, carbon saturated cutting, and modifications of the tool and workpiece materials, in which vibration-assisted machining has been found to be the most promising machining technology.

Elliptical vibration cutting (EVC) was proposed by Shamoto and Moriwaki [6], which is a cutting process where a cutting tool moves along an elliptical path generated by adding the cyclic vibrations on the cutting tool in the cutting and the chip flow directions. Because of the excellent machining performances over conventional cutting (CC) and one-dimensional vibration cutting (1-DVC), EVC has been used in the machining of die steel materials, and very good machining results have been achieved. Shamoto et al. [7] succeeded in applying EVC to the ultra-precision turning of hardened die steel, in which the machining performances in cutting force, surface finish, and tool life were significantly improved, and a spherical mirror surface was obtained. In addition, Shamoto

et al. [8] developed a controller for the vibration device to improve the vibration locus, and a mirror surface with better surface quality was achieved on hardened die steel. Moreover, Zhang et al. [9] investigated the machinability of hardened steel by applying EVC with polycrystalline diamond (PCD) tools, and a mirror-like surface was obtained instead of using single crystal diamond (SCD) tools.

Some researchers have proposed the amplitude control method to machine the micro/nano structures on hardened steel with EVC. Suzuki et al. [10] succeeded in sculpturing various sophisticated microstructures on hardened steel using EVC by controlling the vibration amplitude in the thrust direction. In addition, Zhang et al. [11] compensated the amplitude control error, and the machining accuracy was enhanced. Controlling the amplitude to achieve the profiles of the microstructures is a great method to apply EVC to the micro/nanostructure machining. In this method, the depth of the generated surface is less than the maximum vibration amplitude in the thrust direction, but the depths of the freeform surfaces are generally much larger than the elliptical vibration amplitudes. Therefore, this method would be not suitable for the freeform surface machining.

In the machining processes applying EVC, the EVC devices are the key components. For the designs of the EVC devices, much research has been done. In general, the EVC devices can be classified into the resonant and the non-resonant types. Figure 1 shows the illustrations of the representative designs of the vibration devices, in which (a)–(d) are the resonant vibration devices and (e)–(f) are the non-resonant vibration devices.

The resonant EVC devices are driven to vibrate at the resonant frequency by the actuators. Brinksmeier et al. [18] and Li et al. [12] utilized the structure asymmetry of the transducer to generate the bending vibration based on the longitudinal vibration, and the combined longitudinal-bended vibration mode creates the elliptical vibration of the cutting tool. In addition, Moriwaki et al. [13] and Shamoto et al. [8] attached piezoelectric plates on the sides of a beam to actuate the beam to vibrate in the two bending directions, generating the elliptical trajectories at the beam end. Furthermore, Suzuki et al. [14] sandwiched the piezoelectric actuators between the metal blocks, and the vibrations of the block end in the longitudinal and bending directions generate the elliptical locus. Moreover, Guo et al. [15] developed a new EVC device based on the design concept of an ultrasonic motor, in which the piezoelectric rings are sandwiched with a flexure head and two end blocks. The vibrations of the head in the tangential and normal directions generate the elliptical locus. In general, the resonant EVC devices can achieve high vibration frequencies, whereas some vibration parameters such as frequency and amplitude cannot be adjusted very conveniently.

On the other hand, some non-resonant EVC devices have been developed. Ahn et al. [19] and Kim et al. [16] utilized two orthogonal linear motions output by two actuators that are placed perpendicular to each other to create elliptical locus. Furthermore, Cerniway et al. [20], Kim et al. [17], and Kim et al. [21] used some intermediate structures to convert two parallel linear motions generated by two actuators that are placed abreast into elliptical trajectory. In general, the non-resonant EVC devices have lower operating frequencies compared with the resonant devices, but the vibration parameters of the devices can be arbitrarily set and adjusted, and the devices can be controlled very conveniently.

Previous designs of the EVC devices mainly concentrated on the generation of the elliptical locus and achieving higher vibration frequency, and the devices were used in the machining of flat surfaces [9, 21], microgrooves [17, 22], microstructures [10, 22, 23], or spherical surfaces [7, 24] with the supplementary motions of the *Z* direction guideway and the rotary

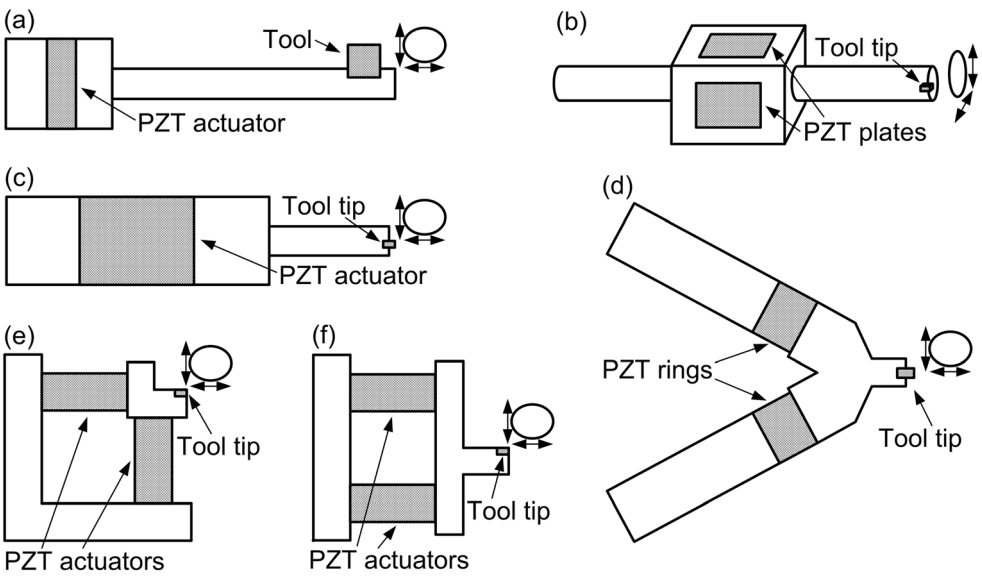

Fig. 1 Illustrations of the representative designs: resonant devices: **a** Li et al.'s design [12]; **b** Moriwaki et al.'s design [13]; **c** Suzuki et al.'s design [14]; **d** Guo et al.'s design [15]; non-resonant devices: **e** Kim et al.'s design [16]; **f** Kim et al.'s design [17]

table applied by the machine tool. But these EVC devices would be not suitable for the freeform surface generation.

The objective of this paper is to propose a new apparatus to apply EVC into the freeform surface machining on die steel materials. The rest of this paper is organized as follows. The principle of the proposed device is explained in Section 2. The device is developed in Section 3, followed by the testing experiments in Section 4, and the freeform surface machining experiments in Section 5. Finally, this paper is concluded with a summary in Section 6.

2 Principle of double-frequency elliptical vibration cutting device

Figure 2a shows the principle of the proposed double-frequency elliptical vibration cutting (DFEVC) device, which combines EVC and FTS. The EVC and FTS parts of the combined device output the high-frequency elliptical vibration to improve the machinability in material removal and the low-frequency oscillations to generate the profiles of the freeform surfaces, respectively.

The operating frequency is a very important parameter for the combined device, which is much influenced by the operating frequencies of the EVC and FTS parts. The frequency of the combined device should be equal to or less than the lower one of the two parts' frequencies. In general, the operating frequencies of the EVC devices are higher than those of the FTS devices. Therefore, the operating frequency of the combined device is determined by the frequency of the FTS part, and the frequency of the EVC part should be equal to or less than the frequency of the FTS part. The EVC part can work at the frequency where the FTS part works, to enable the combined device to achieve the highest possible frequency. Since the two parts work at the same frequency, the *Z* direction vibration of the EVC part can be conducted by the FTS part to simplify the device design, as shown in Fig. 2b.

3 Development of a double-frequency elliptical vibration cutting device

3.1 Design of mechanical structure

As reviewed in the introduction part, the vibration devices can be classified into the resonant type and the non-resonant type. Compared with the resonant vibration devices, the non-resonant vibration devices are easier to control and some parameters can

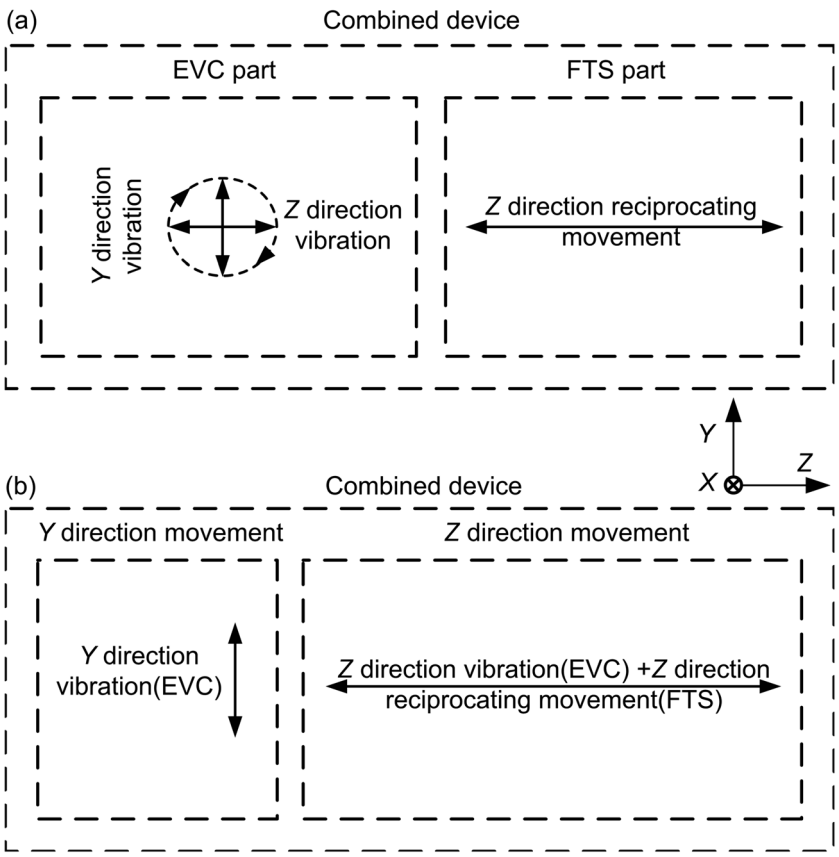

Fig. 2 Principle of the DFEVC device: **a** combination of EVC and FTS, **b** simplification of the combination

be set arbitrarily. For the non-resonant vibration devices, the ellipse generation of the devices with two orthogonal actuators is more simple and direct, and the motion control is more convenient, compared with those devices with two parallel actuators. In addition, the precision control for the displacement outputs of the device is highly required in the freeform surface machining. Therefore, the non-resonant vibration device structure with two orthogonal actuators is selected to design the double-frequency elliptical vibration cutting device.

Figure 3 shows the mechanical structure of the designed device. To avoid the installation error between the hinge part and the base part, the two parts are designed to be an integral flexure hinge structure. The integral flexure part is made from 65Mn steel, and other parts 45 steel. The Z direction actuator pushes a block to drive the Z direction moving part. Inside the Z direction moving part are the Y direction actuator and the Y direction moving part, on which the cutting tool is mounted.

The guide mechanisms are designed to be parallel and symmetric structures using flexure hinges. The Z direction moving part is guided by the Z direction flexure mechanism, which consists of twelve parallel elastic hinges. The Y direction moving part is guided by the Y direction flexure mechanism with four parallel elastic hinges. When the Z direction actuator drives the Z direction moving part to move along a straight line in the Z direction, the Y direction moving part generates the same movements. On the other hand, the Y direction actuator directly drives the Y direction moving part to move in the Y direction. Because of the parallelity and symmetry of the guide mechanisms, when the moving parts are driven, the tool on the Y direction moving part outputs translational motions, in which the angle of the tool rake face does not change.

The stiffness of the guide mechanisms in the directions of movements is a very important parameter. Figure 4a shows one layer of the guide mechanisms. Figure 4b shows the displacements and deformations of the hinge structure when a force $2F$ is imposed on midpoint C, which can be considered as a statically indeterminate beam [25, 26]. After removing the constraints at C and adding the restraint moment M, the loads and deformations of the hinge structure are shown in Fig. 4c. The displacement in the direction of movement and the rotation angle at B can be calculated as below:

$$d_B = -\frac{Fl^3}{3EI} - \frac{Fal^2}{2EI} + \frac{Ml^2}{2EI} \tag{1}$$

$$\theta_B = -\frac{Fl^2}{2EI} - \frac{Fal}{EI} + \frac{Ml}{EI} \tag{2}$$

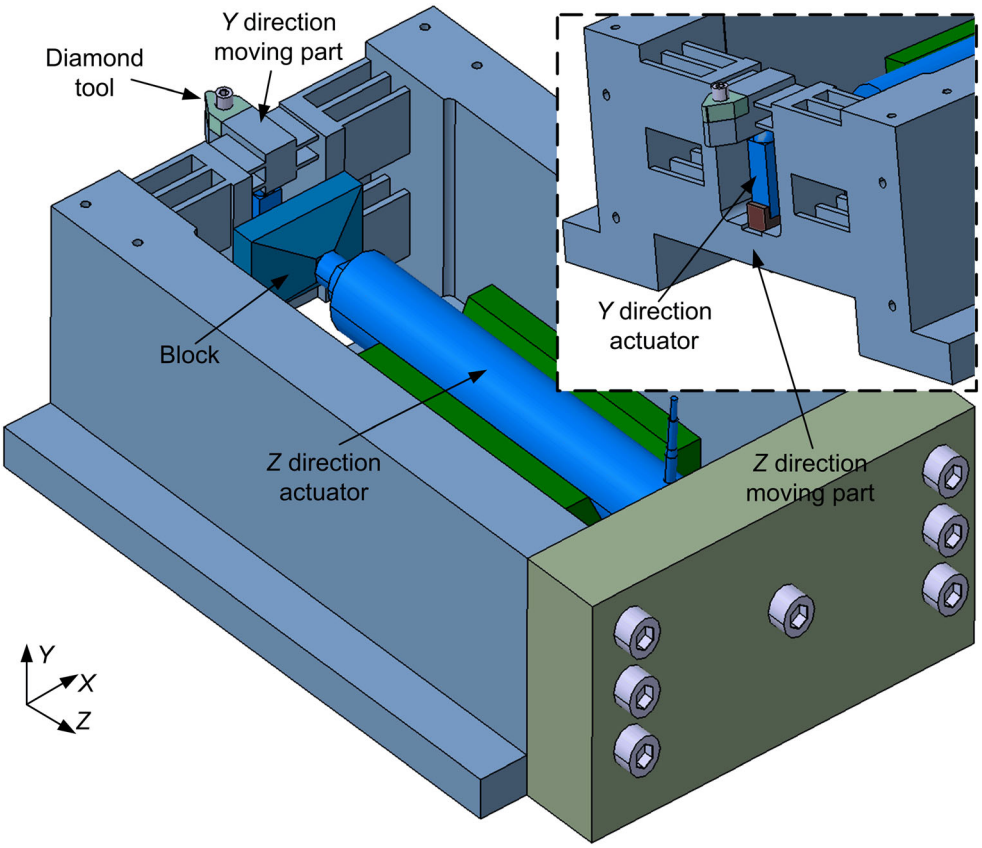

Fig. 3 Mechanical structure of the DFEVC device

where E is the young's modulus of the hinge material, and I is the moment of inertia, which can be calculated as below:

$$I = \frac{bt^3}{12} \tag{3}$$

where b is the width, and t is the thickness of the hinge.

The moving body BD is set to be rigid, therefore the boundary condition below can be found:

$$\theta_B = 0 \tag{4}$$

Based on Eqs. (2) and (4), M can be derived as below:

$$M = F\left(\frac{l}{2} + a\right) \tag{5}$$

Substituting Eq. (5) to Eq. (1), the displacement at B can be obtained as below:

$$d_B = -\frac{Fl^3}{12EI} \tag{6}$$

Therefore, the stiffness along the direction of movement can be calculated as below:

$$k = \left|\frac{2F}{d_C}\right| = \left|\frac{2F}{d_B}\right| = \frac{24EI}{l^3} = \frac{2Ebt^3}{l^3} \tag{7}$$

Therefore, the Z direction stiffness of the Z direction guide mechanism can be obtained as below:

$$K_Z = 6k_Z \tag{8}$$

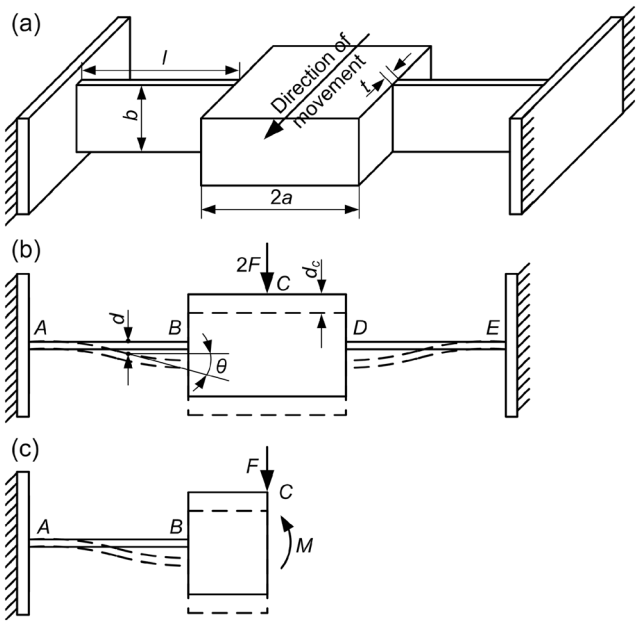

Fig. 4 Stiffness calculation: **a** single layer of the flexure mechanism, **b** top view of the hinge structure under the load in the direction of movement, and **c** loads and deformations of the hinge structure

where k_Z is the Z direction stiffness of one layer of the Z direction flexure mechanism, which can be calculated as $k_Z = \frac{2Eb_Zt_Z^3}{l_Z^3}$.

Similarly, the Y direction stiffness of the Y direction guide mechanism can be calculated as below:

$$K_Y = 2k_Y \tag{9}$$

where $k_Y = \frac{2Eb_Yt_Y^3}{l_Y^3}$.

Table 1 gives the main structure parameters of the designed flexure structures, and the stiffness of the guide mechanisms calculated following the formulas above.

3.2 Actuator and sensor for the designed device

Two piezoelectric actuators are used to drive the flexure mechanisms. The Z direction actuator, 145 mm in length and 19.8 mm in outer diameter, has a stroke of 90 um, axial stiffness of 38 N/μm, and a maximum output force of 3000 N. The Z direction actuator pushes a block to drive the Z direction moving part. The Y direction actuator has a stroke of 15 μm, axial stiffness of 100 N/μm, and a maximum output force of 1750 N. It has a small size of 7 × 7 × 21.5 mm, which is installed inside the Z direction moving part.

A capacitive displacement sensor with a resolution of 1 nm and a bandwidth up to 100 kHz is used to measure the tool displacements in the Z and Y directions for the feedback control of the tool motions. Two probes of the sensor are fixed on the top cover of the device to obtain the displacements of the Y direction moving part in the two directions, which can be considered as the displacements of the cutting tool mounted on it, because of its translational motions.

4 Testing experiments

Figure 5 shows the designed vibration device and the instruments, including a PID controller, a capacitive displacement sensor, and a charge amplifier for the following testing experiments. The control signals from the controller are amplified

Table 1 The main parameters of the designed flexure mechanisms

Parameters	Values
b_Z	16 mm
t_Z	2.0 mm
l_Z	22 mm
K_Z	28.85 N/μm
b_Y	15 mm
t_Y	0.8 mm
l_Y	7 mm
K_Y	17.91 N/μm

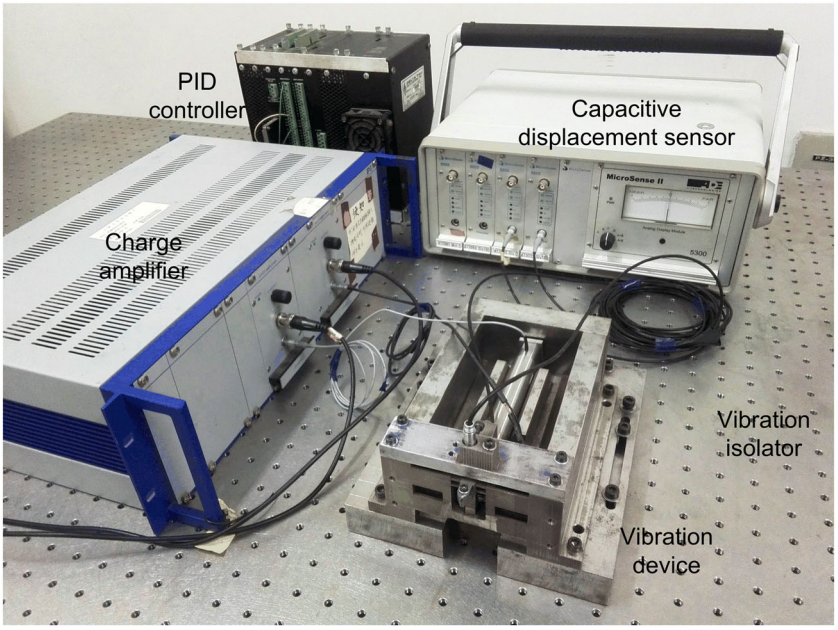

Fig. 5 Vibration device and experimental instruments

by the amplifier, and then given to the actuators to drive the device. The displacement sensor passes the measured displacement data of the cutting tool to the controller for the closed-loop control of the tool motions.

4.1 Stiffness

The stiffness of the *Z* direction and the *Y* direction flexure mechanisms in the directions of movements are measured as 27.59 and 18.44 N/μm, respectively, which are very close to the results from the theoretical calculations, 28.85 and 17.91 N/μm.

4.2 Sinusoidal sweep response

A sinusoidal sweep signal with continuously changing frequencies is applied to the *Z* direction actuator, and the displacement response in the *Z* direction is recorded and analyzed by fast Fourier transformation (FFT). The results are shown in Fig. 6a, in which the frequency at the first peak corresponding to the first resonance frequency is 1257.74 Hz. A sinusoidal sweep signal is applied to the *Y* direction actuator to test the resonance frequency in the *Y* direction, and the first resonance frequency in the *Y* direction can be found as 1896.19 Hz from the curve shown in Fig. 6b. The resonance frequencies are large enough to carry out the freeform surface machining experiments.

4.3 Closed-loop tracking and crosstalk

The positioning capability of the device system is a significant performance parameter, which is highly relevant to the machining accuracy of freeform surfaces. For the designed two-degree-of-freedom device, the positioning accuracy of the device system and the influences of the output displacements in the two directions on each other should be tested and identified.

A 40-$\mu m_{p\text{-}p}$ sinusoidal wave signal is given to the *Z* direction actuator under the closed-loop control, and the displacement responses in the two directions are shown in Fig. 7. The maximum following error in the *Z* direction is 0.6 μm, which is 1.5 % of the full testing stroke (40 μm). Meanwhile, the maximum displacement in the *Y* direction can be found as 0.06 μm, which is 0.6 % of the *Y* direction testing stroke (10 μm) in the next experimental process.

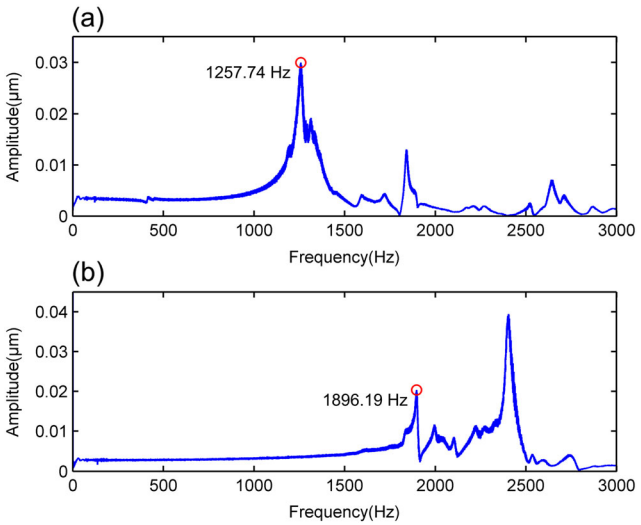

Fig. 6 FFT of sinusoidal sweep responses: **a** in the *Z* direction and **b** in the *Y* direction

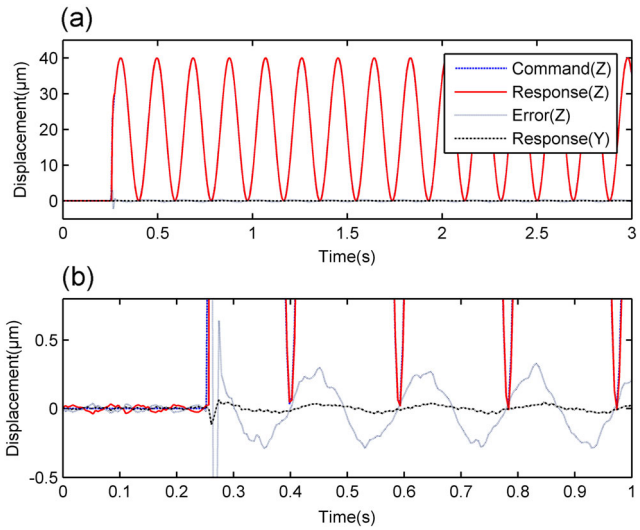

Fig. 7 Tracking results in the *Z* direction: **a** displacement responses, **b** partial enlarged drawing

Figure 8 shows the tracking results when the *Y* direction actuator is commanded by a sinusoidal wave signal with an amplitude of 10 $\mu m_{p\text{-}p}$. The maximum following error in the *Y* direction is less than 0.2 μm, which is 2 % of the testing stroke (10 μm). The displacement in the *Z* direction can be found almost the same as that before the tracking test, which can be nearly considered as the noise and ignored.

The following errors in the two directions are both acceptable, and the influences of the motions in the two directions on each other are both very slight.

4.4 Resolution

A stair control voltage is given to the *Z* direction actuator, and the displacements in the *Z* direction are recorded and plotted in Fig. 9a, from which the resolution can be found as 8 nm. The resolution in the *Y* direction is tested in a similar way, which can be found as less than 8 nm from Fig. 9b.

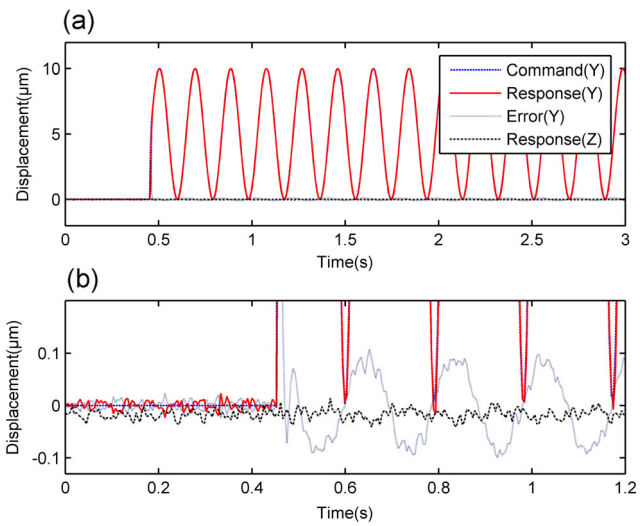

Fig. 8 Tracking results in the *Y* direction: **a** displacement responses, **b** partial enlarged drawing

4.5 Elliptical trajectory generation

Two sinusoidal signals 4 $\mu m_{p\text{-}p}$ in amplitude with phase shifts of 0°, 45°, 90°, 135°, and 180° at frequencies ranging from 10 to 150 Hz are applied to the two actuators, and the vibration centers of the signals given to the *Z* and *Y* direction actuators are 18 and 2 μm, respectively.

Figure 10 shows the resultant ellipses with different phase shifts and frequencies. The ellipses are precisely generated at 10 Hz. As the frequency increases, the errors in the two directions rise, and the error in the *Z* direction is smaller than that in the *Y* direction. At around 50 Hz, the ellipses can be accurately generated with slight distortion. At around and above 100 Hz, the error in the *Z* direction does not change much, while the increase of the error in the *Y* direction is obvious and the *Y* direction amplitudes become smaller, but the shapes of the ellipses are still regular.

Actually, in the machining process, the *Z* direction end tips of the elliptical trajectories generate the surface profiles. As the frequency increases, the *Y* direction amplitude decreases, and the tips move towards the *Y* direction vibration center, 2 μm. But the tip locations of the ellipses with 90° phase shift almost do not change, just with smaller amplitudes in the *Y* direction. Figure 11a, b shows the surface generation processes at the same vibration frequency, in which the amplitude in (b) is smaller than that in (a). It can be found that the surface roughness increases when the *Y* direction amplitude decreases.

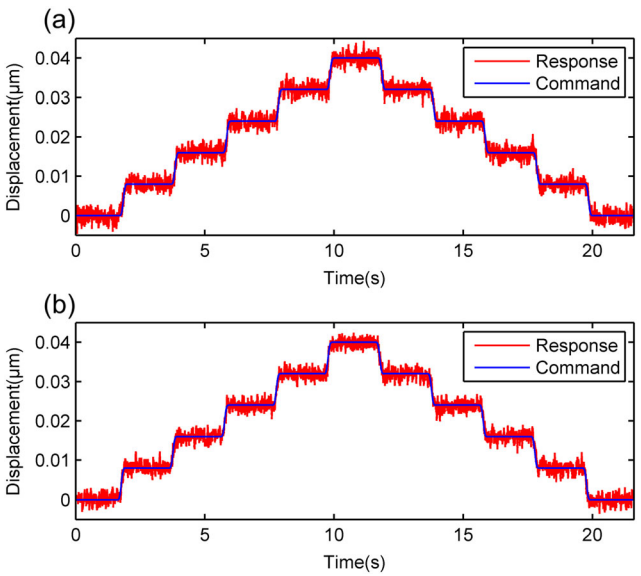

Fig. 9 Resolutions in the two directions: **a** in the *Z* direction and **b** in the *Y* direction

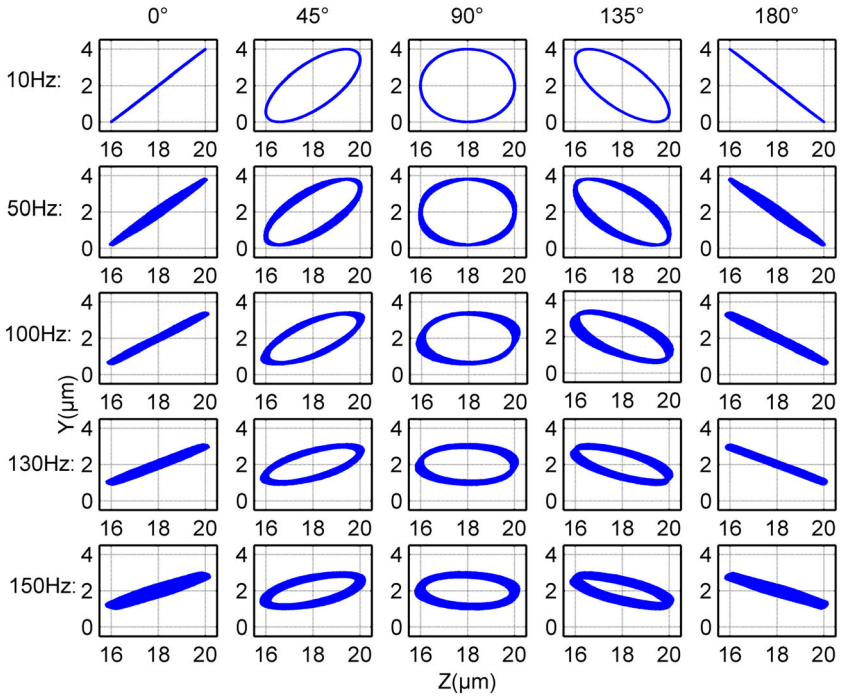

Fig. 10 Resultant ellipses with different phase shifts and frequencies

The roughness can be improved by selecting other parameters suitably. Actually, the decrease of the Y direction vibration amplitude occurs at around and above 100 Hz, the influence of which on the roughness can be offset and even improved by the increased frequencies, as shown in Fig. 11c, d.

At around 50 Hz, the elliptical trajectories with high control accuracy can be obtained. At around 100 Hz, the ellipses with a 90° phase shift also can be used in the machining, and smaller roughness can be achieved than that at lower frequencies.

4.6 Double-frequency elliptical vibration tracking

To generate the elliptical vibration and the low-frequency oscillations, two driving signals are applied to the Z and Y direction actuators, respectively:

$$\begin{cases} z(t) = 2\sin(2\pi f_v t) + 8\sin(2\pi f_s t) + 10 \\ y(t) = 2\sin(2\pi f_v t + \varphi) + 2 \end{cases} \tag{10}$$

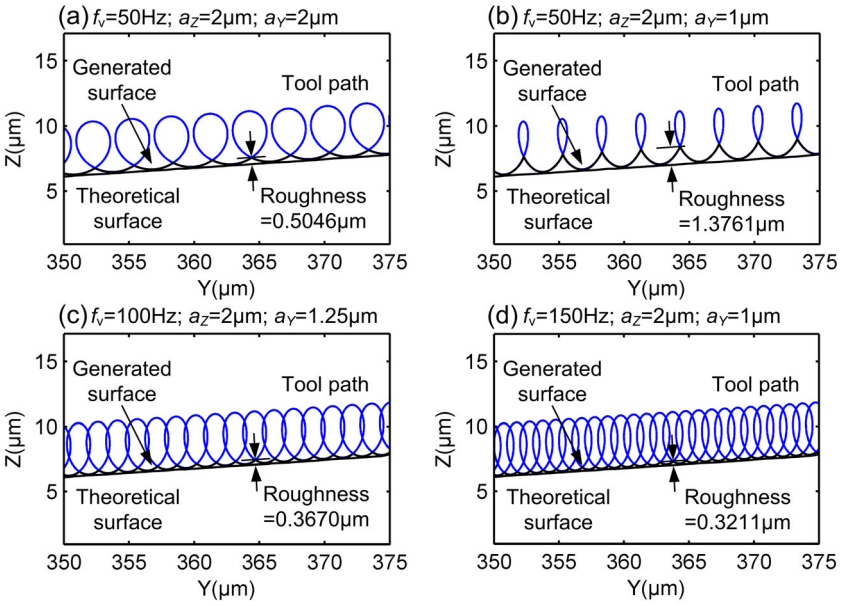

Fig. 11 Surface generation processes under different Y direction amplitudes and frequencies

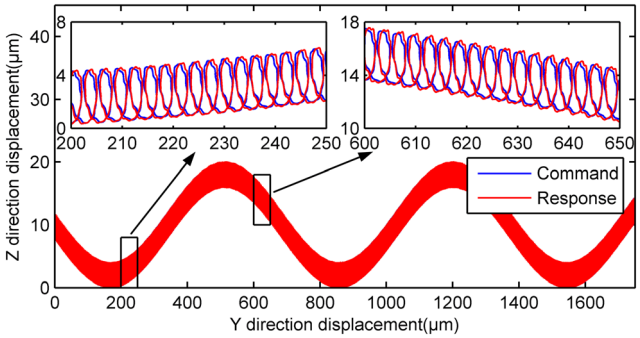

Fig. 12 Resultant tool paths

where f_v is the frequency of the elliptical vibration, f_s is the frequency of the oscillations corresponding to the freeform surface, and φ is the phase shift.

Figure 12 shows the resultant tool paths under the cutting speed of 150 μm/s, in which the freeform profiles are enveloped by the elliptical trajectories.

The resultant tool paths with different phase shifts under the cutting speed of 150 μm/s are shown in Fig. 13. The paths with phase shifts of 0° and 180° cannot envelop the profiles very well for the large surface roughness of the enveloped profiles. In addition, the wavy paths will result in the instability of the cutting process, which is not conducive to the conduct of material removal in the machining process. Therefore, the elliptical trajectories with 0° and 180° phase shifts are not suitable for the freeform surface machining, and the trajectories with other phase shifts can be selected according to the requirements of the machining parameters.

Figure 14 shows the resultant tool paths at different frequencies with 150 μm/s cutting speed and 90° phase shift. As the vibration frequency increases, the profiles in Fig. 14b are enveloped very well, which are smoother than those in Fig. 14a, although the elliptical paths deform. At the higher oscillation frequency, the profiles also can be well enveloped as shown in Fig. 14c, and the increased errors of the generated profiles are acceptable.

The testing results show that the device system can generate the elliptical vibration and the oscillations corresponding to the profiles of the freeform surfaces very well, which is consistent with the proposed principle and indicates this device system can apply EVC into the freeform surface machining.

5 Machining experiments and discussions

5.1 Experimental system

The machining experiments of the freeform surfaces are carried out on the SPINNER precision lathe. As shown in Fig. 15, the vibration device is mounted on the *X* direction guideway, and the workpiece is clamped by the chuck of the spindle. During the machining process, the workpiece rotates at a constant speed, and the vibration device moves along the *X* direction. Meanwhile, the vibration device is commanded by the controller to output the tool movements to generate the surface profiles.

The machining parameters are shown in Table 2. In the testing experiments, the profiles enveloped by the double-frequency elliptical vibration at around 100 Hz have better surface finish than those enveloped at around 50 Hz, although the elliptical trajectories at around 100 Hz have slightly lower control accuracy than those at around 50 Hz. Therefore, the vibration frequency of 100 Hz is used in the machining experiments. In addition, the phase shift is set to 90°, based on the analysis in the testing experiments. 40Cr die steel is selected as the workpiece material, which is widely used in the manufacture of molds and mechanical elements.

Fig. 13 Resultant tool paths with different phase shifts

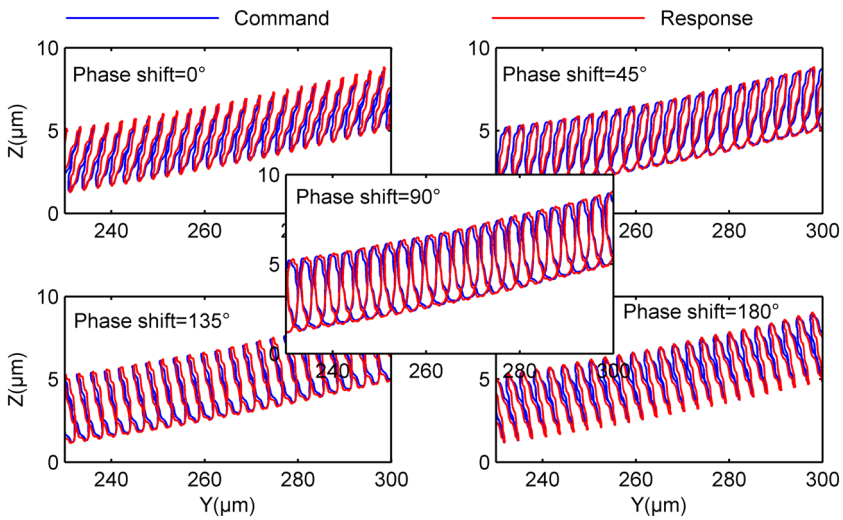

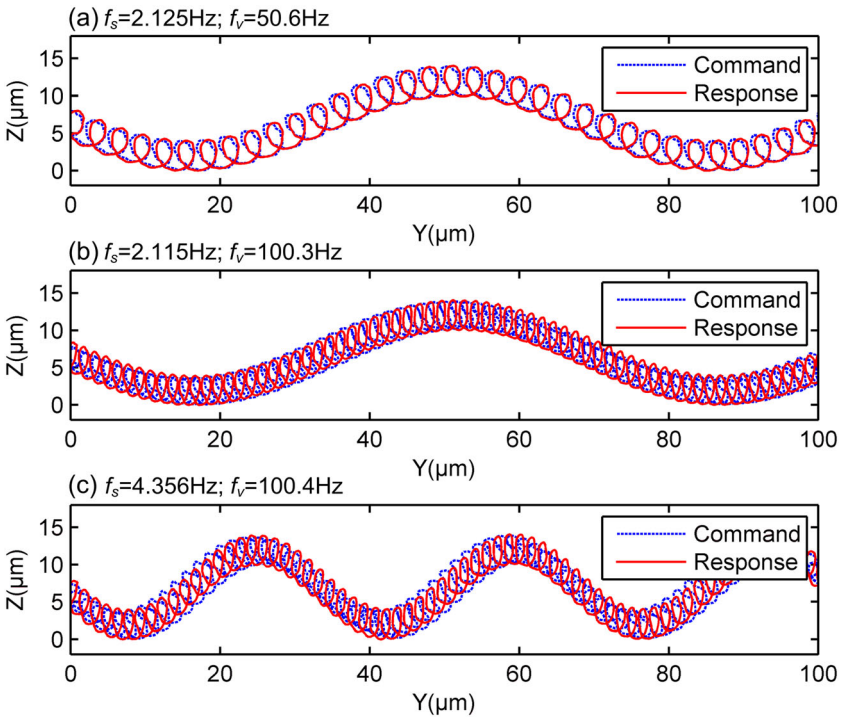

Fig. 14 Resultant tool paths at different frequencies

5.2 Machining results and discussions

Two workpieces 20 mm in diameter are used in the experiments, and the sinusoidal wavy surfaces are generated on the central regions 5 mm in diameter of the workpieces with different machining methods. One is machined by the conventional FTS method, and the other is by the DFEVC method. When the workpiece is machined by the conventional FTS method, the DFEVC device just outputs the oscillations, while the device outputs the oscillations and the elliptical vibration when applying the DFEVC method. Figure 16a, b shows the simulated sinusoidal wavy surface to be machined. The machined surfaces by the conventional FTS method and the DFEVC method are shown in Fig. 16c, d, respectively.

Figure 17 shows the comparisons between the surfaces machined by conventional FTS and DFEVC, in which the areas are corresponding to the areas marked in Fig. 16b. Figure 17a1 shows the machining results of area A by conventional FTS, in which the 2-D and 3-D images of the surface and the measured profile along the feed direction are on the

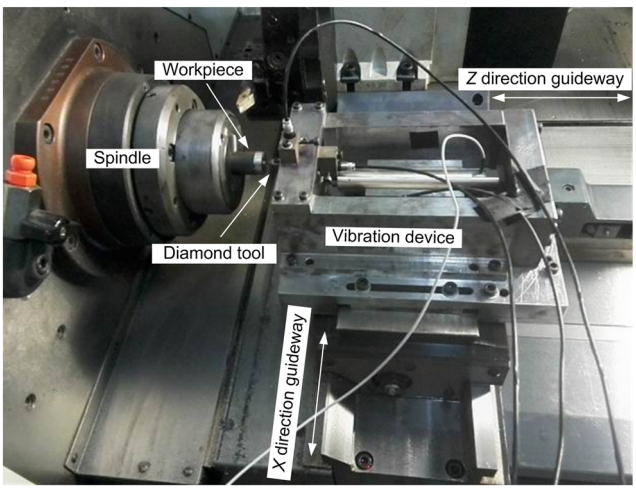

Fig. 15 Machining system

Table 2 The machining parameters used in the surface generation

Turning conditions	Spindle rotation speed	6 rev/min
	Feed rate	25 μm/rev
	Depth of cut	10 μm
Vibration conditions	*Y* direction amplitude	2 μm
	Z direction amplitude	2 μm
	Phase shift	90°
	Frequency	100 Hz
Sinusoidal wavy surface	Amplitude	10 $\mu m_{p\text{-}p}$
	Wavelength	1000 μm
Workpiece	Material	40Cr steel
	Diameter	20 mm
Tool	Material	Polymer crystal diamond
	Nose radius	0.3 mm
	Rake angle	0°
	Clearance angle	10°

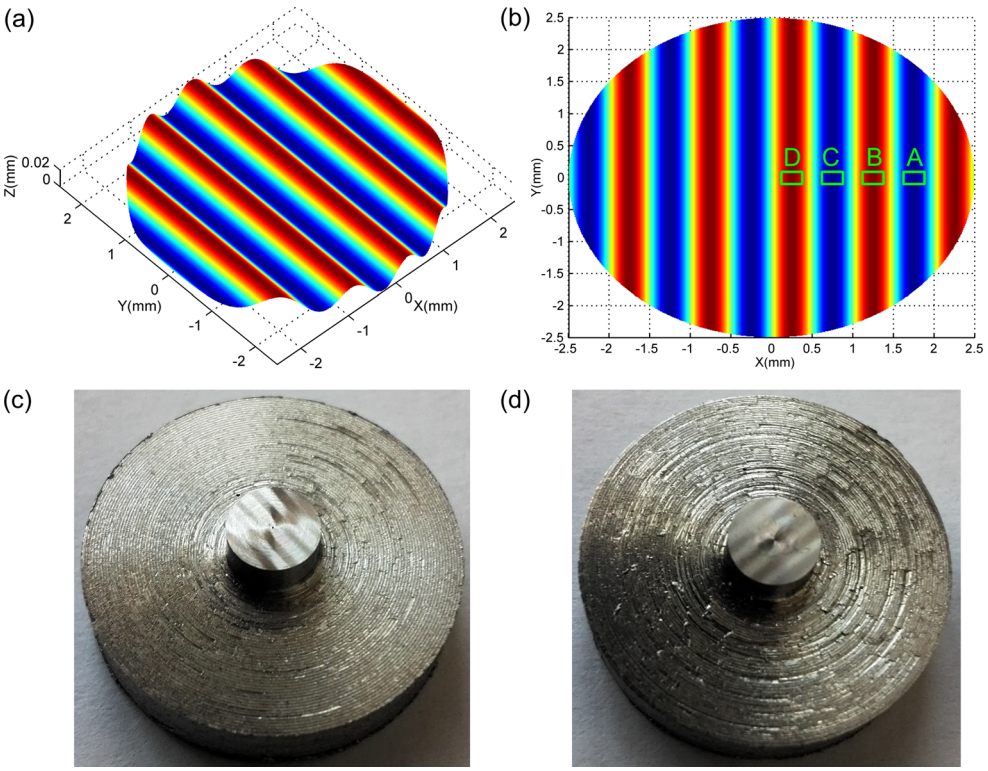

Fig. 16 **a** Simulation of a sinusoidal wavy surface. **b** *XOY* view of the surface. **c** Surface generated by the conventional FTS method. **d** Surface generated by the DFEVC method

left side, and the measured results of the enlarged central region of area A are given on the right side. Some tear and scratches can be observed on the machined surfaces, which deteriorate the surface finish. In addition, it can be found from the measured profiles that the deep scratches degrade the form accuracy of the surfaces. The machining results of area A by DFEVC are shown in Fig. 17a2, and the feed marks and the vibration marks along the cutting direction can be observed, which are considered as the characteristics of diamond turning and EVC, respectively. The vibration marks result in rough surfaces, but almost no tear and scratches are observed on the surfaces. The profiles show better form accuracy than the results by conventional FTS.

Figure 17b1, b2 shows the machining results of area B by the two methods. Some tear and scratches still can be observed on the surfaces machined by conventional FTS, which are detrimental to the surface finish and the form accuracy. Better surfaces without tear and scratches are achieved by DFEVC, and the vibration marks are less obvious than those shown in Fig. 17a2.

Figure 17c1, c2 shows the machining results of area C. Compared with area B shown in Fig. 17b1, more tear and scratches are observed on the surfaces machined by conventional FTS in Fig. 17c1, which severely deteriorate the surface quality. The feed and the slight vibration marks can be observed on the surfaces machined by DFEVC in Fig. 17c2, without tear and scratches, and the profiles show better form accuracy than those shown in Fig. 17c1.

Figure 17d1, d2 shows the measured results of area D. Some tear and periodic groves can be observed on the surfaces generated by conventional FTS, which significantly damage the surface finish. In addition, it can be found from the measured profiles that the deep grooves result in the catastrophic deterioration of the form accuracy of the machined surfaces. The surfaces machined by DFEVC are very smooth and fine, with the periodic and slight feed marks, and almost no vestiges of the vibration marks. The surface quality is much better than that of the surfaces machined by conventional FTS shown in Fig. 17d1.

In different locations of the surface machined by conventional FTS, the tear and scratches deteriorate the surface finish and the form accuracy of the surfaces. Because of the tear and the scratches, the feed marks of the machined surfaces cannot be clearly identified. As the cutting process continues, the deep scratches and grooves severely degrade the surface integrity and the form accuracy. On the other hand, almost no tear and scratches are observed on the surfaces machined by DFEVC, and the surfaces with better surface quality and form accuracy are achieved. The feed and vibration marks can be observed, which are generated by the feed and the elliptical vibration of the cutting tool, respectively. As the machining process proceeds, the vibration marks become smaller and smaller. Actually, the tool marks can be further improved by selecting more suitable machining parameters.

Compared with conventional FTS, the introduction of the elliptical vibration effectively improves the machinability in

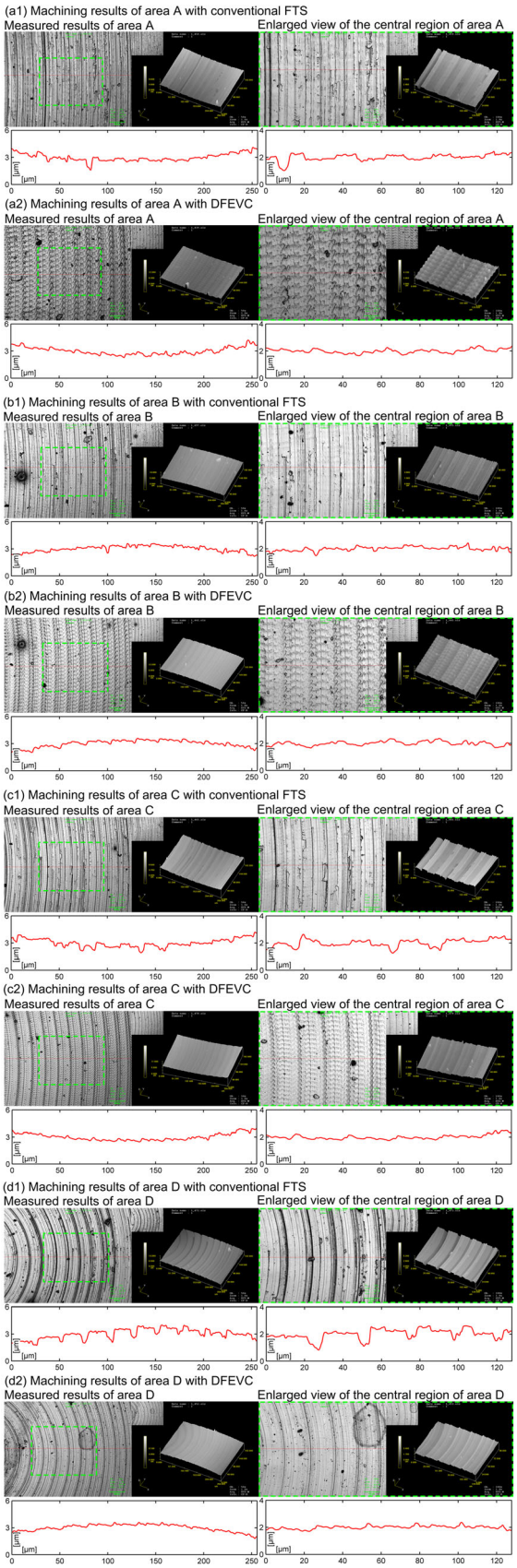

Fig. 17 Comparisons of the surfaces machined by conventional FTS and DFEVC

processing die steel, which helps DFEVC to achieve the freeform surfaces with much better processing quality.

6 Conclusions

In this paper, a new apparatus has been proposed for the freeform surface diamond machining on die steel materials. The apparatus has been designed, analyzed, and verified. The following conclusions can be drawn from this study:

(1) The DFEVC apparatus combines EVC for the improvement of the machinability in material removal and FTS for the profile generation of freeform surfaces, to achieve the freeform surface diamond machining on die steel materials.
(2) The apparatus outputs the elliptical vibration and the oscillations in the cutting process, and the resultant tool path envelops the profiles of freeform surfaces with the overlapping elliptical trajectories.
(3) The freeform surface machined by the DFEVC method shows much better surface integrity and form accuracy than that machined by the conventional FTS method, which validates the feasibility of the principle and the DFEVC apparatus.

Acknowledgments The authors are grateful to the financial support from the National Natural Science Foundation of China (51175221; 51375060; 51075041; 51305162), and the Department of Science and Technology of Jilin Province (20130522155JH).

References

1. Fang FZ, Zhang XD, Weckenmann A, Zhang GX, Evans C (2013) Manufacturing and measurement of freeform optics. CIRP Ann Manuf Technol 62(2):823–846. doi:10.1016/j.cirp.2013.05.003
2. Patterson SR, Magrab EB (1985) Design and testing of a fast tool servo for diamond turning. Precis Eng 7(3):123–128. doi:10.1016/0141-6359(85)90030-3
3. Dow TA, Miller MH, Falter PJ (1991) Application of a fast tool servo for diamond turning of nonrotationally symmetric surfaces. Precis Eng 13(4):243–250. doi:10.1016/0141-6359(91)90001-Y
4. Li ZJ, Fang FZ, Gong H, Zhang XD (2013) Review of diamond-cutting ferrous metals. Int J Adv Manuf Technol 68(5):1717–1731. doi:10.1007/s00170-013-4970-5
5. Paul E, Evans CJ, Mangamelli A, McGlauflin ML, Polvani RS (1996) Chemical aspects of tool wear in single point diamond turning. Precis Eng 18(1):4–19. doi:10.1016/0141-6359(95)00019-4
6. Shamoto E, Moriwaki T (1994) Study on elliptical vibration cutting. CIRP Ann Manuf Technol 43(1):35–38. doi:10.1016/S0007-8506(07)62158-1
7. Shamoto E, Moriwaki T (1999) Ultaprecision diamond cutting of hardened steel by applying elliptical vibration cutting. CIRP Ann Manuf Technol 48(1):441–444. doi:10.1016/S0007-8506(07)63222-3
8. Shamoto E, Suzuki N, Moriwaki T, Naoi Y (2002) Development of ultrasonic elliptical vibration controller for elliptical vibration

cutting. CIRP Ann Manuf Technol 51(1):327–330. doi:10.1016/S0007-8506(07)61528-5
9. Zhang XQ, Kumar AS, Rahman M, Nath C, Liu K (2011) Experimental study on ultrasonic elliptical vibration cutting of hardened steel using PCD tools. J Mater Process Technol 211(11):1701–1709. doi:10.1016/j.jmatprotec.2011.05.015
10. Suzuki N, Yokoi H, Shamoto E (2011) Micro/nano sculpturing of hardened steel by controlling vibration amplitude in elliptical vibration cutting. Precis Eng 35(1):44–50. doi:10.1016/j.precisioneng.2010.09.006
11. Zhang J, Suzuki N, Wang Y, Shamoto E (2015) Ultra-precision nano-structure fabrication by amplitude control sculpturing method in elliptical vibration cutting. Precis Eng 39:86–99. doi:10.1016/j.precisioneng.2014.07.009
12. Li X, Zhang D (2006) Ultrasonic elliptical vibration transducer driven by single actuator and its application in precision cutting. J Mater Process Technol 180(1–3):91–95. doi:10.1016/j.jmatprotec.2006.05.007
13. Moriwaki T, Shamoto E (1995) Ultrasonic elliptical vibration cutting. CIRP Ann Manuf Technol 44(1):31–34. doi:10.1016/S0007-8506(07)62269-0
14. Suzuki N, Haritani M, Yang J, Hino R, Shamoto E (2007) Elliptical vibration cutting of tungsten alloy molds for optical glass parts. CIRP Ann Manuf Technol 56(1):127–130. doi:10.1016/j.cirp.2007.05.032
15. Guo P, Ehmann KF (2013) Development of a tertiary motion generator for elliptical vibration texturing. Precis Eng 37(2):364–371. doi:10.1016/j.precisioneng.2012.10.005
16. Kim GD, Loh BG (2008) Characteristics of elliptical vibration cutting in micro-V grooving with variations in the elliptical cutting locus and excitation frequency. J Micromech Microeng 18(2):025002
17. Kim GD, Loh BG (2007) An ultrasonic elliptical vibration cutting device for micro V-groove machining: kinematical analysis and micro V-groove machining characteristics. J Mater Process Technol 190(1–3):181–188. doi:10.1016/j.jmatprotec.2007.02.047
18. Brinksmeier E, Gläbe R (1999) Elliptical vibration cutting of steel with diamond tools. In: Proc. of the 14th Annual ASPE Meeting, Monterey, California, vol 05.11
19. Ahn J-H, Lim H-S, Son S-M (1999) Improvement of micro-machining accuracy by 2-dimensional vibration cutting. In: Proc ASPE, p 150–153
20. Cerniway MA (2002) Elliptical diamond milling: kinematics, force and tool wear
21. Kim H-S, Kim S-I, Lee K-I, Lee D-H, Bang Y-B, Lee K-I (2009) Development of a programmable vibration cutting tool for diamond turning of hardened mold steels. Int J Adv Manuf Technol 40(1–2):26–40
22. Kim GD, Loh BG (2010) Machining of micro-channels and pyramid patterns using elliptical vibration cutting. Int J Adv Manuf Technol 49(9–12):961–968
23. Lu Y, Guo P, Pei P, Ehmann K (2015) Experimental studies of wettability control on cylindrical surfaces by elliptical vibration texturing. Int J Adv Manuf Technol 76(9–12):1807–1817. doi:10.1007/s00170-014-6384-4
24. Song Y, Park C-H, Moriwaki T (2010) Mirror finishing of Co–Cr–Mo alloy using elliptical vibration cutting. Precis Eng 34(4):784–789. doi:10.1016/j.precisioneng.2010.02.003
25. Gere JM, Goodno BJ (2009) Mechanics of materials. Seventh edn. Cengage Learning, USA
26. Nie Y, Meng G (2004) Mechanics of materials (in Chinese), 1st edn. China Machine Press, Bei Jing